Numerical Simulation and Reduced Order Model (ROM) of a Thermoacoustic Heat Engine

Fatih Selimefendigil

Department of Mechanical Engineering, Celal Bayar University
Muradiye, Manisa, TR-45140, Turkey
fatih.selimefendigil@cbu.edu.tr

In this study, numerical simulation results and a reduced order model of thermoacoustic heat engine with proper orthogonal decomposition are presented. The governing equations are solved with a finite volume based solver. The reduced order model is obtained using proper orthogonal decomposition taking snapshots when the system reaches limit cycle. The evolution of the pressure, heat transfer from heated parallel plates (stack) to the fluid and flow field at the ends of the stack are presented. A reduced order model with 11-POD modes is obtained for the full system from the Galerkin projection. A polynomial quadratic ODE system is obtained and the effect of neglecting the second order contributions is also presented in this study.

1 Introduction

Thermo-acoustic heat engines which convert heat into acoustic power are widely used in engineering due to their simple design and compact structures with no moving parts. One main problem associated with thermoacoustic heat engines are their low thermal efficiencies. Rayleigh criterion [1] explains thermal to acoustic conversion in a thermo-acoustic heat engine. To understand the transforming mechanism between thermal energy and acoustic energy, numerical and analytical models have been developed for thermoacoustic systems [2–7].

The simulation of thermoacoustic engines requires expensive computations due to their different length and time scales. CFD simulation of thermoacoustic systems have been performed by many researchers. Hantschk and Vortmeyer [8] have performed CFD computations of thermoacoustic in a Rijke tube with heating bands kept at constant temperature. They showed that self-excited oscillations are observed if the Rayleigh criterion is satisfied and limit cycle amplitude is determined by the nonlinearities in the heat flux from the heating element to the flow. Zink et al. [9] have performed a CFD analysis of a whole thermoacoustic engine the influence of a curved resonator on the thermoacoustic effect was investigated. They observed that the introduction of curvature affects the pressure amplitude achieved and severely curved resonators also exhibited a variation in operating frequency. Yu et al. [10] have used CFD method to investigate nonlinear phenomena and processes of a 300 Hz standing wave thermoacoustic engine. The acoustic fields were given, and the vortices evolution in both ends of the stack along which a temperature gradient was imposed were investigated.

For thermo-acoustic systems, prediction and control of thermal to acoustic conversion is an important design objective. Low order modeling of thermo-acoustic systems has become important since a reduction in the computational demand (time and resources) is achieved. Toffolo et al. [11] have presented a methodology to reduce the computational cost of thermoacoustic oscillations. Their procedure suggests the use of CFD calculations for their capability on acoustic aspects rather than on fluid

dynamic details. They lower the computational effort by restraining domain boundaries or by increasing cell dimensions and time steps. Song et al. [12] have presented a CFD-CAA combined method to predict the thermoacoustic instability limit curve. In this approach, the response function for pulsating release of heat in the Rijke tube and the distribution of mean density in the tube are computed with CFD and used as inputs to CAA predictions. There exist also studies where the a model for the heat source is obtained and used in full thermo-acoustic simulations [13–17]. In this approach, a nonlinear model of the heat source may be computationally costly due to curse of dimensionality [17].

In the present study, a reduced order model of a heat engine is presented with the Proper Orthogonal Method (POD). To the best of the authors' knowledge, a low computational effort of the coupled thermoacoustic system with POD has never been reported in the literature.

2 Standing Wave Heat Engine and Numerical Model

Rayleigh criterion [1] explains thermal to acoustic conversion in a thermo-acoustic heat engine which consists of heat cavity, heat exchangers and stack. A detail for the one of the pores in the stack (parallel plates) is shown on the right part of Fig.1. A gas parcel at (A) rejects heat to the cold heat exchanger, and at (B) it is compressed with the acoustic wave. At (C), it takes heat from the hot heat exchanger and at (D), it starts to expand. A net positive work is obtained as the area under the P-v diagram of the thermodynamic cycle. The phase between the heat transfer and the acoustic oscillation is obtained with the thermal diffusion.

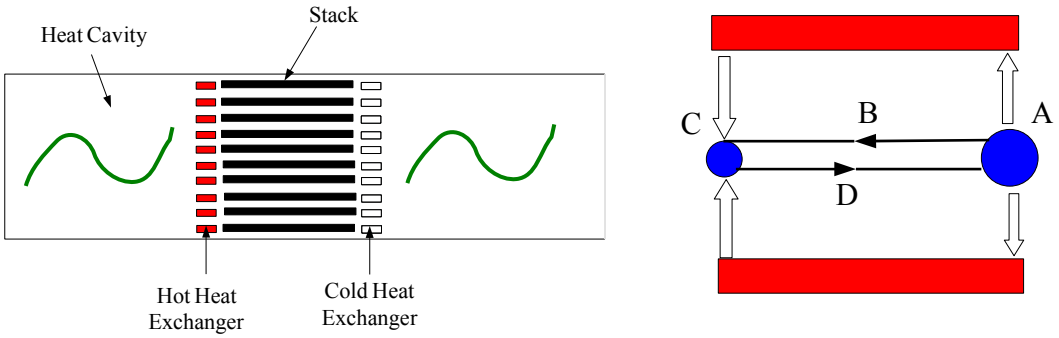

Figure 1: A thermo-acoustic prime mover with heat exchangers and stack (left), a detail for one of the pores in the stack along with a gas parcel experiencing expansion and compression (right)

A schematic description of the problem is shown in Fig.2 (a). It is a simple standing wave engine and a stack of parallel heated plates located in the vicinity of the closed end. Our model problem is similar to the one considered in [9]. It is 150 mm (=L) long and 51(=H) mm wide in dimensions. The stacks are placed 30 mm (=x_f) from the downstream of the closed end and are given a non-zero thickness. The length of the stack along which a temperature gradient imposed is 10 mm (=b) and the spacing between the stacks are 0.25 mm (=d).

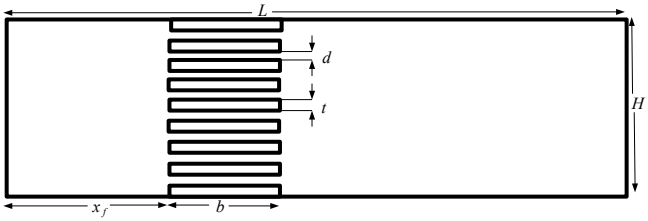

(a) Geometry

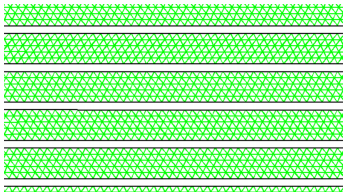

(b) Detail of mesh

Figure 2: Geometry of the heat engine and a detail of the mesh in the vicinity of the stack

Governing equations, boundary conditions and solution method

The conservation equations for mass, momentum and energy are solved in 2d case for a laminar compressible flow with Fluent are :

$$\frac{\partial \rho}{\partial t} + \frac{\partial (\rho v_x)}{\partial x} + \frac{\partial (\rho v_y)}{\partial y} = 0, \tag{1}$$

$$\frac{\partial (\rho \mathbf{v})}{\partial t} + \nabla . (\rho \mathbf{v}\mathbf{v}) = -\nabla p + \nabla . (\tau), \tag{2}$$

$$\frac{\partial (\rho E)}{\partial t} + \nabla . \left(\mathbf{v} (\rho \mathbf{E} + \mathbf{p})\right) = \nabla . [k \nabla T + (\tau . \mathbf{v})], \tag{3}$$

where ρ, v, p, τ, E denote the density, velocity, pressure, stress tensor and energy, respectively. and k represent the dynamic viscosity and thermal conductivity, respectively. The state equation of an ideal gas is used which is given as

$$p = \rho RT. \tag{4}$$

The model of the thermoacoustic heat engine has an open end and pressure inlet to create a pressure gradient and non-zero velocity field in the computational domain. The stack walls are at constant temperature with a given temperature gradient from 700 K to 300 K over the stack length. The outer wall of the heat engine is assumed to be adiabatic. A zero velocity boundary condition was used for all walls. Equations (1-3) along with the boundary and initial conditions are solved with a finite volume based commercial CFD code (FLUENT). Second order upwind scheme is used for spatial discretization. PISO algorithm is used for velocity-pressure coupling and second order implicit time differencing is utilized. A time step of 10^{-5} is decided to be sufficient to obtain results independent of time step size. For the unsteady calculation, the pressure inlet boundary condition is replaced with an adiabatic wall [9]. Mesh independence study is also carried out to obtain an optimal grid distribution with accurate results and minimal computational time. The number of the triangular cells used in computations is 46392. The mesh is finer near the edges of the stack walls and in the spacing separating the stack plates to resolve the high gradients of the field variables there. A detail of the mesh is shown in Fig.2 (b).

3 Proper Orthogonal Decomposition for compressible flow

An ensemble of data set, either from numerical simulations or experiments, can be expressed in terms of a reduced order basis. The fluctuating part of the data set is expressed as a linear combination of spatial eigenfunction multiplied with time dependent coefficients as:

$$q(x,t) = \bar{q}(x) + \sum_{i=1}^{N_m} a_i(t)\Phi_i(x) \tag{5}$$

In the above equation, the data set is truncated with N_m number of modes.

The modes will then be calculated by minimizing the distance between the original data and approximated (projected) data [18]

$$\left|\left|q - \text{Projection}(q)\right|\right| \rightarrow \text{MIN.} \tag{6}$$

This is equivalent to maximizing the inner product of ensemble average, normalized by the inner product of the basis vectors [18],

$$\frac{\langle (q,\Phi)^2 \rangle}{(\Phi,\Phi)} \rightarrow \text{MAX.} \tag{7}$$

For two vector field variables $\vec{r}$ and $\vec{s}$, the inner product is the defined as the integration of their scalar product over the domain V,

$$(\vec{r},\vec{s}) = \int_V \sum_{l=1}^{L} r_l s_l \, dV. \tag{8}$$

The expression in Eq.(7) can be then reformulated as an integral eigenvalue problem.

$$\int_V \langle q(x) \bigotimes q(x') \rangle \, \Phi(x') \, dx' = \lambda \Phi(x). \tag{9}$$

As it has been shown by Rowley et al. [19], an energy based inner product will lead to stability of the Galerkin system (after projection) around the linearization point. Another aspect is the nondimensionalisation when we use vectorial form of the flow variables. Without nondimensionalisation, the standard inner product may not be the suitable choice because of dimensional consistency. One can nondimensionalise the flow variables, but the optimality of the projection depends on the nondimensionalisation [19]. Bourguet et al. [20] have defined a specific scaled inner product (weighted spatial product) to ensure POD-dimensional consistency [20]. This approach in [20] is also adopted in this study.

3.1 POD - Galerkin Projection

The vector of variables for compressible flow denoted by q are defined in [20] assuming constant viscosity as

$$q = \left[1/\rho, v_1, v_2, p\right]' \tag{10}$$

Using the data set in terms of POD modes (truncated with N_m - POD modes) and the orthogonality of the POD modes, a quadratic form of the ODE in terms of time dependent modal coefficients are obtained from compressible Navier-Stokes equations as,

$$\frac{da_i(t)}{dt} = \sum_{k=1}^{N_m}\sum_{j=1}^{N_m} A1_{ijk} a_k(t) a_j(t) + \sum_{j=1}^{N_m} A2_{ij} a_j(t) + A3_i. \tag{11}$$

A_1, A_2 and A_3 are constant coefficients issued from Galerkin projection. They are functions of POD modes and their spatial derivatives.

4 Results and Discussion

In the following, the results from CFD will be presented and a reduced order model of the full thermoacoustic system in limit cycle oscillations will be obtained using POD method.

4.1 CFD results

Fig.3 shows the time evolution of absolute pressure oscillation and a detail of the periodic state state oscillation (limit cycle). It is seen that the pressure oscillation starts from an initial disturbance until the balance between the acoustic power dissipation and acoustic power generation is reached. The frequency of the oscillation is 618 Hz which is in good agreement with the result of [9]. Fig.4 shows the pressure fluctuation and heat transfer fluctuation (heat transfer from heated plates to the fluid elements) in the limit cycle. It is seen that the maximum of the pressure does not coincide with the maximum of heat flux but with a phase advance due to the thermal inertia. The Rayleigh criterion is met in this case.

Fig.5 shows the three points during the acceleration phase of a period. Flow field at the end of the stacks are shown in Fig.6 at the time instances according to Fig.5. The flow field is directed towards the negative x direction at the time instances a and b, while it is directed towards positive x direction at point c (at the time instance where the pressure reaches maximum value). From point a towards point b, the magnitude and the intensity of the flow field at the left and right part of the stacks increase. Entrance effect is observed at the right part of the stack at points a and b and at the left part of the stack at point c. The flow field then changes periodically. The axial temperature distribution for the time points according to Fig.5 where the axis is located at $y = 0.0028$ m is shown in Fig.7. In this plot, the location of the stack is also plotted with vertical lines. With the time increment from point a towards point c, the location of the peak value of the temperature shifts towards the closed end. The magnitude of the temperature increases outside the stack and remains below the temperature value in the stack when moving from point a towards point c.

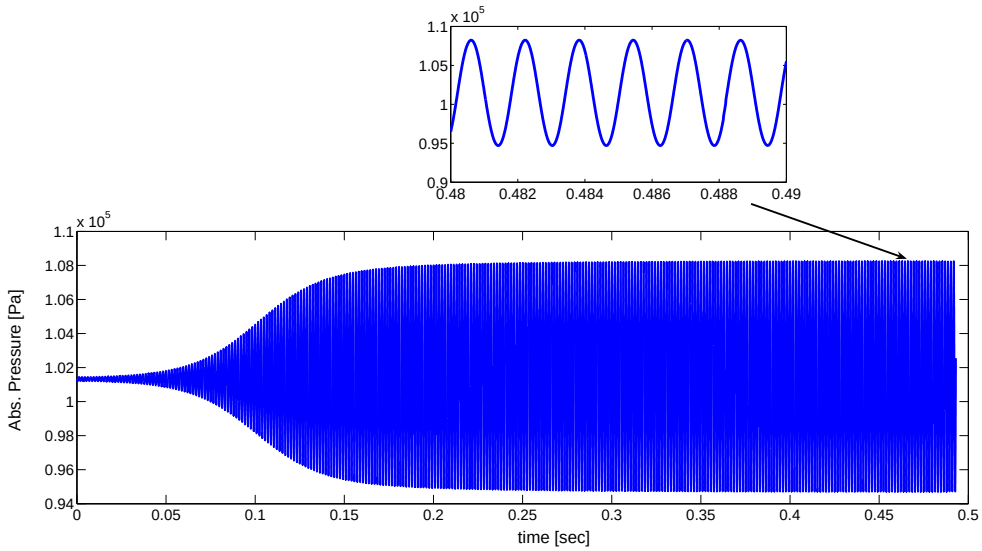

Figure 3: Time evolution of the pressure oscillations and a detail of the oscillation in the limit cycle at a point in the vicinity of the stack.

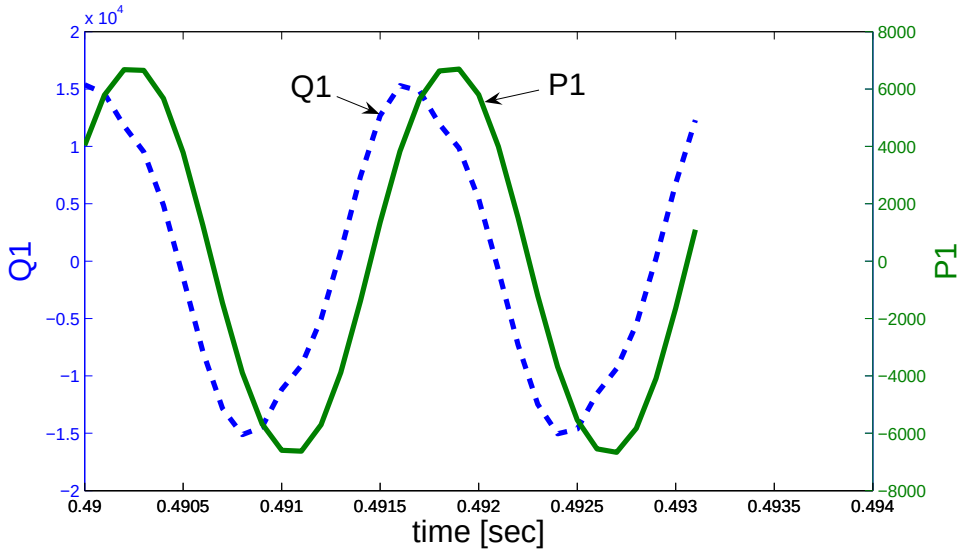

Figure 4: Calculated simulation results in the limit cycle for pressure and heat transfer from the heated plates to the fluid at a point in the vicinity of the stack.

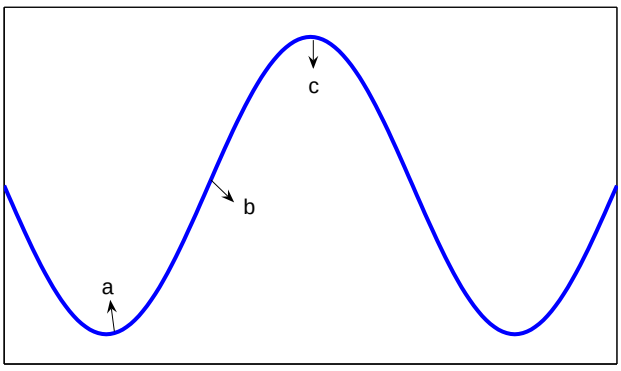

Figure 5: Three points during the acceleration phase of a period

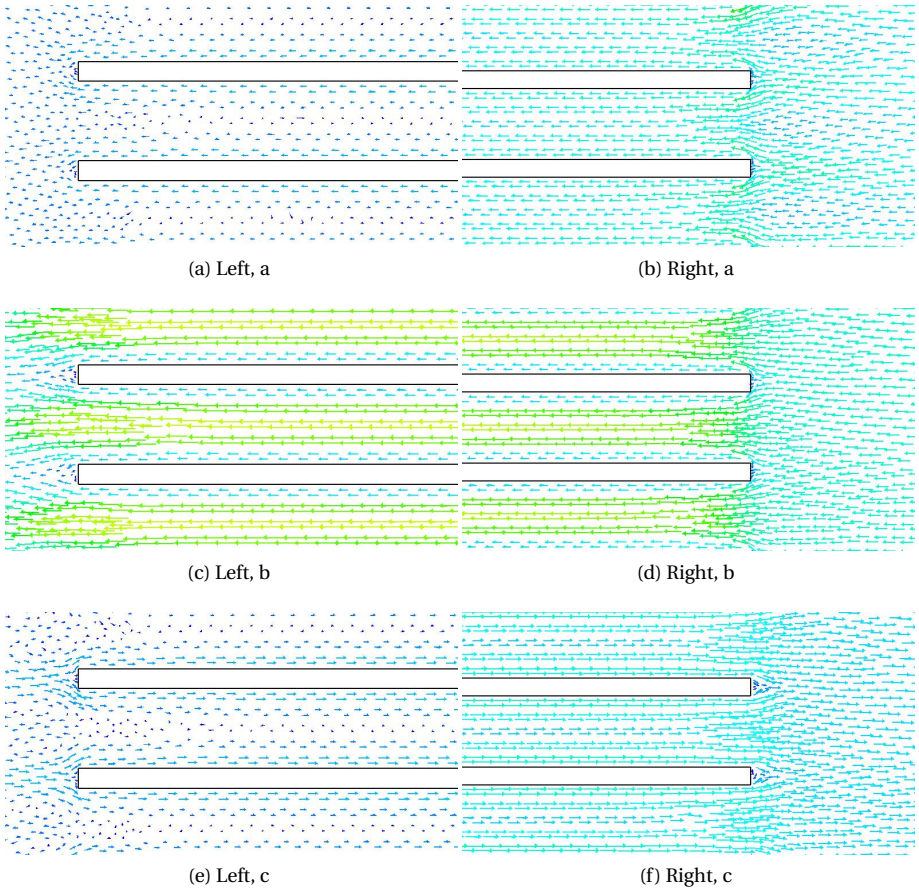

(a) Left, a (b) Right, a

(c) Left, b (d) Right, b

(e) Left, c (f) Right, c

Figure 6: Flow field as vectorial plots in the ends of the stack for the time instances according to Fig.3

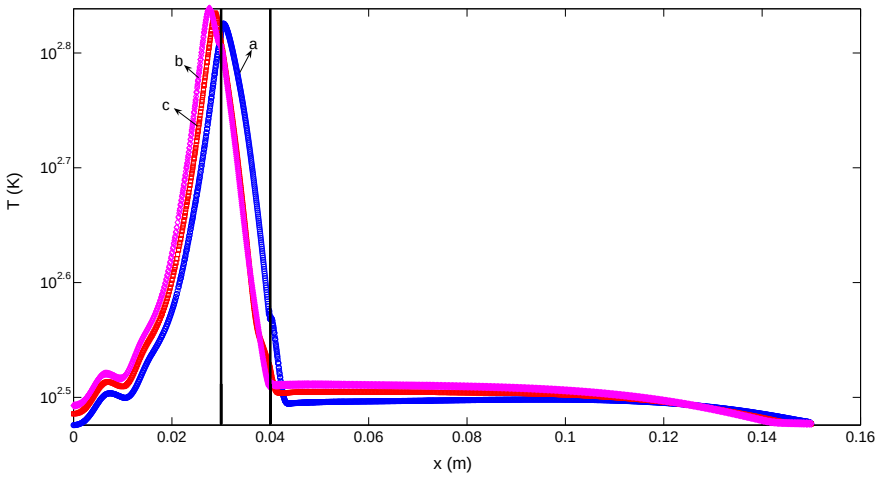

Figure 7: Temperature distribution along the horizontal axis located at $y = 0.0028$ m for the time instances according to Fig.3.

4.2 POD results

The POD base is extracted when the limit cycle is reached for $M = 33$ snapshots from equally spaced time interval with a time step of $10\Delta t$. The relative magnitude of the eigenvalue gives a measure for the statical content of the corresponding POD mode. The cumulative modal contribution is also defined as

$$\text{Modal contribution} = \frac{\sum_{i=1}^{N_m} \sigma_i}{\sum_{i=1}^{M} \sigma_i} \tag{12}$$

As it is shown in Fig.8, 11 POD modes capture more than 99.9 percentage of the snapshot series statistical content.

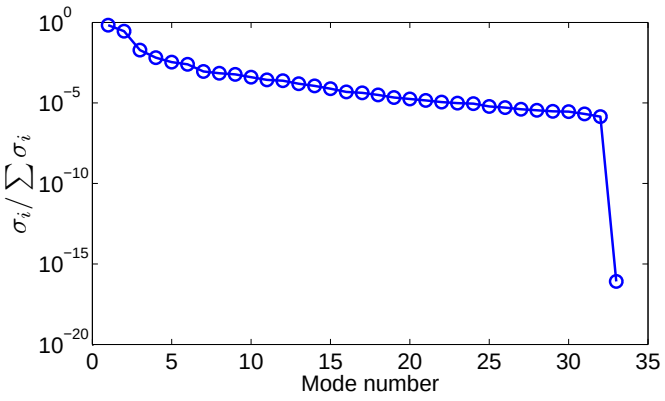

(a)

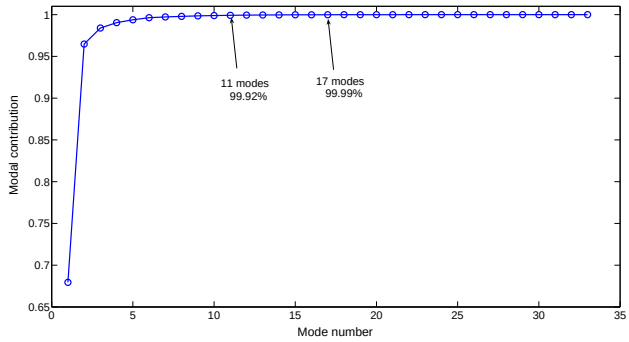

(b)

Figure 8: Relative energy content of each mode (a) and modal contribution of the truncated POD basis (b).

Reference temporal evolutions of modal coefficients are obtained by projecting the data set onto the POD modes. In Fig. 9, the reference modal coefficients are shown in continuous lines for mode numbers between 1 to 9. The effect of omitting the nonlinear contribution in Eq.11 is also illustrated in these plots. Neglecting the second order nonlinear terms in Eq.11 have effects on higher index modes. The amplitude and phase drifts are observed when neglecting these terms as indicated by square shaped markers in Fig.9. A second order ODE model which is illustrated in circle markers in Fig.11, captures very well the reference modal coefficients. The reduced order model integration is performed by using a four-stage Runge-Kutta scheme. The phase diagrams in Fig.10 shows the predicted modal coefficients both for neglecting the second order term and retaining it when the periodic regime is reached. The final amplitude of the limit cycle agrees well with the data from CFD for the second order ODE model.

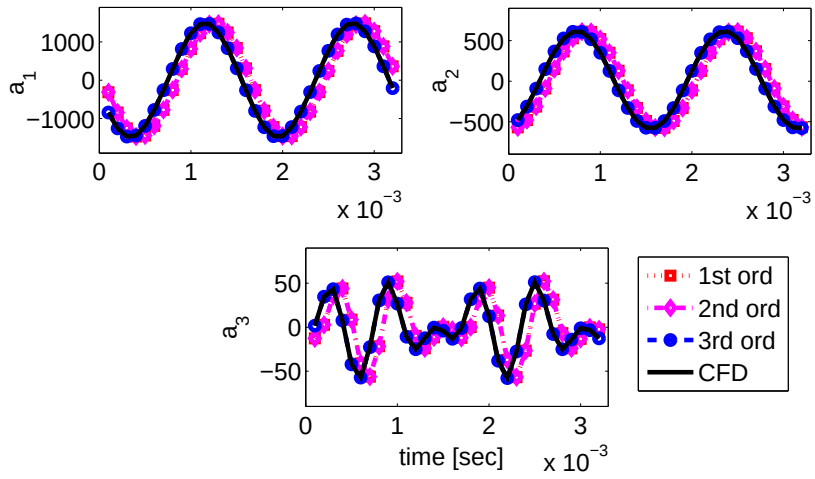

(a) Modes 1-3

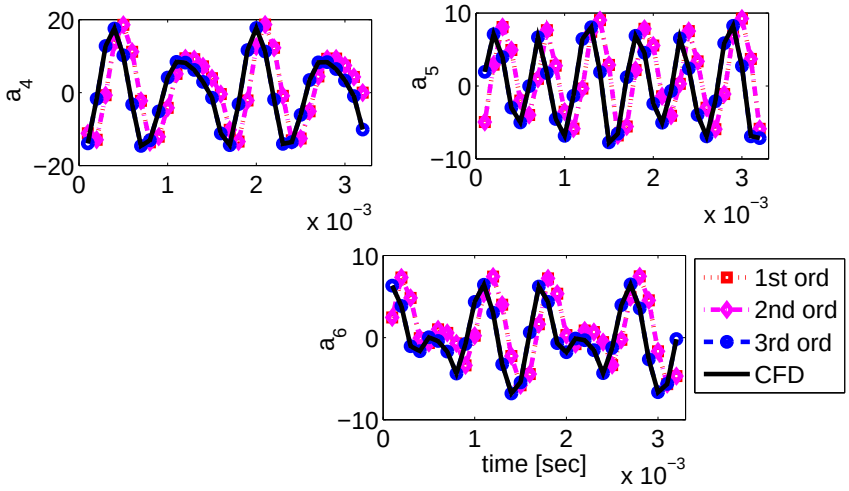

(b) Modes 4-6

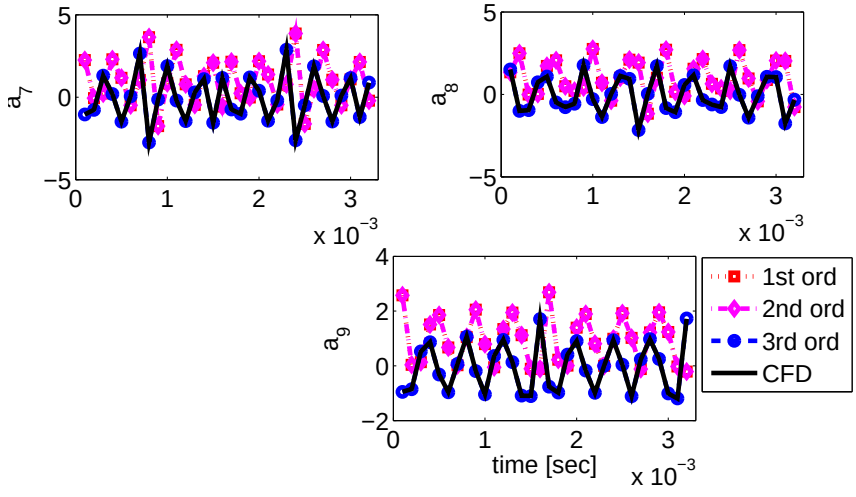

(c) Modes 7-9

Figure 9: Time evolution of the POD modal coefficients from CFD (reference values), neglecting and retaining second order terms.

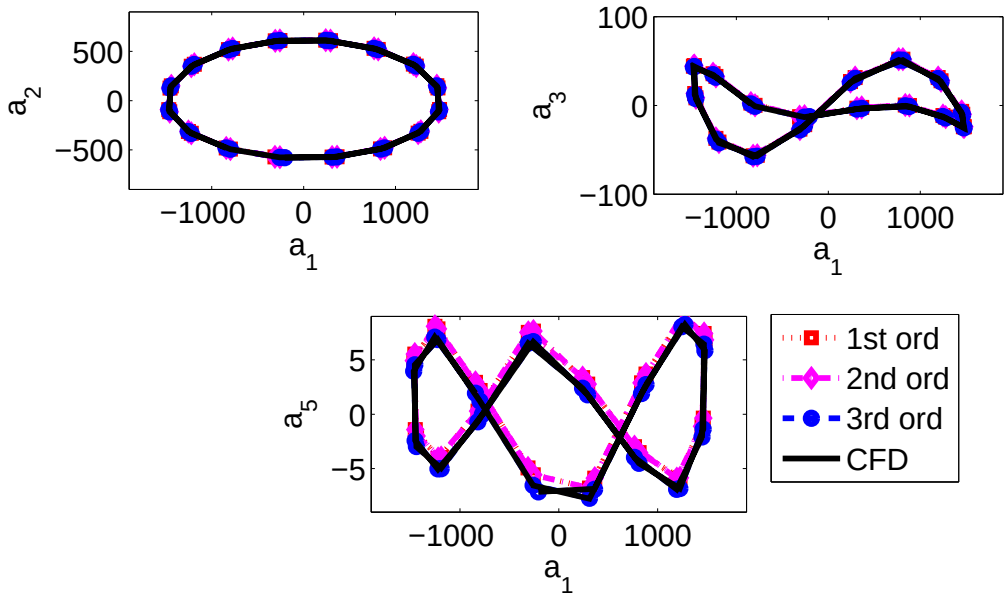

Figure 10: POD-ROM prediction in the phase space when the limit cycle is reached.

5 Conclusions and Outlook

In the present study, numerical simulation of a standing wave thermoacoustic heat engine is performed and a POD based reduced order of the system is presented. Following results are obtained:

- The maximum of the pressure does not coincide with the maximum of heat flux but with a phase advance due to the thermal inertia and the Rayleigh criterion is met in this case.
- A reduced order model (quadratic ODE system) with 11 modes are obtained with POD after Galerkin projection.
- Neglecting the second order nonlinear terms in ODE have effects on higher index modes. The amplitude and phase drifts are observed when neglecting these terms.
- The reduced order model procedure can be extended to investigate the effects of a parameter variation, e.g., stack location on the limit cycle oscillation which will be the subject of our next paper.

References

[1] J. W. S. Rayleigh. The explanation of certain acoustical phenomena. *Nature*, 181:319–321, 1878.

[2] A. P. Dowling. Nonlinear self-excited oscillations of a ducted flame. *J. of Fluid Mechanics*, 346:271–290, 1997.

[3] F. E. C. Culick. Non-linear growth and limiting amplitude of acoustic oscillations in combustion chambers. *Combust. Sci. and Tech.*, 3:1–16, 1971.

[4] W. Polifke. Low-order analysis tools for aero- and thermo-acoustic instabilities. In C. Schram, editor, *Advances in Aero-Acoustics and Thermo-Acoustics*. Van Karman Institute for Fluid Dynamics., Rhode-St-Genèse, Belgium, 2010.

[5] W. Polifke. System identification for aero- and thermo-acoustic applications. In C. Schram, editor, *Advances in Aero-Acoustics and Thermo-Acoustics*. Van Karman Inst for Fluid Dynamics., Rhode-St-Genèse, Belgium, 2010.

[6] N. Noiray, D. Durox, T.Schuller, and S. Candel. A unified framework for nonlinear combustion instability analysis based on the flame describing function. *J. of Fluid Mechanics*, 615:139–167, 2008.

[7] Haruko Ishikawa and David J. Mee. Numerical investigations of flow and energy fields near a thermoacoustic couple. *J. Acoust. Soc. Am.*, 111:831–839, 2002.

[8] C. Hantschk and D. Vortmeyer. Numerical simulation of self-excited thermoacoustic instabilities in a rijke tube. *J. of Sound and Vibration*, 3(277):511–522, 1999.

[9] Florian Zink, Jeffrey Vipperman, and Laura Schaefer. Cfd simulation of a thermoacoustic engine with coiled resonator. *International Communications in Heat and Mass Transfer*, 37:226–229, 2010.

[10] Guoyao Yu, W. Dai, and Ercang Luo. Cfd simulation of a 300 hz thermoacoustic standing wave engine. *Cryogenics*, 50:615–622, 2010.

[11] Andrea Toffolo, Massimo Masi, and Andrea Lazzaretto. Low computational cost cfd analysis of thermoacoustic oscillations. *Applied Thermal Engineering*, 30:544–552, 2010.

[12] Woo-Seog Song, Seungbae Lee, , and Dong-Shin Shin. Prediction of thermoacoustic instability in rijke tube using cfd-caa numerical method. *Journal of Mechanical Science and Technology*, 25:675–682, 2011.

[13] L. Tay Wo Chong, T. Komarek, R. Kaess, S. Föller, and W. Polifke. Identification of Flame Transfer Functions from LES of a Premixed Swirl Burner. In *Proceedings of ASME Turbo Expo 2010*, number GT2010-22769, Glasgow, Scotland, 2010.

[14] W. Polifke and C. O. Paschereit. Determination of thermo-acoustic transfer matrices by experiment and computational fluid dynamics. *ERCOFTAC Bulletin*, 38, September 1998.

[15] W. Polifke, A. Poncet, C. O. Paschereit, and K. Döbbeling. Reconstruction of acoustic transfer matrices by instationary computational fluid dynamics. *J. of Sound and Vibration*, 245:483–510, 2001.

[16] F. Selimefendigil, R.I. Sujith, and W. Polifke. Identification of heat transfer dynamics for non-modal analysis of thermoacoustic stability. *Applied Mathematics and Computation*, 217:5134–5150, 2011.

[17] F. Selimefendigil, S. Föller, and W. Polifke. Nonlinear identification of the unsteady heat transfer of a cylinder in pulsating crossflow. *Computers and Fluids*, 53:1–14, 2012.

[18] V. Lenaerts, G. Kerschen, and J. C. Golinval. Proper orthogonal decomposition for model updating of non-linear mechanical systems. *Mechanical Systems and Signal Processing*, 15(1):31–43, 2001.

[19] C. W. Rowley, T. Colonius, and R. Murray, M. Model reduction for compressible flows using pod and galerkin projection. *Physica D*, 189:115–129, 2004.

[20] R. Bourguet, Braza M., and A. Dervieux. A. reduced-order modeling for unsteady transonic fows around an airfoil. *Phys. Fluids*, 19:1–4, 2007.